NRL Report 7886

Monte Carlo Calculations of Neutron and Photon Spectra for the INDI Project

G. H. HERLING

Theory Branch
Radiation Technology Division

June 10, 1975

NAVAL RESEARCH LABORATORY
Washington, D.C.

UNCLASSIFIED

REPORT DOCUMENTATION PAGE

READ INSTRUCTIONS BEFORE COMPLETING FORM

1. REPORT NUMBER: NRL Report 7886	2. GOVT ACCESSION NO.
3. RECIPIENT'S CATALOG NUMBER	
4. TITLE (and Subtitle): MONTE CARLO CALCULATIONS OF NEUTRON AND PHOTON SPECTRA FOR THE INDI PROJECT	5. TYPE OF REPORT & PERIOD COVERED: Final report on one phase of the NRL problem.
	6. PERFORMING ORG. REPORT NUMBER
7. AUTHOR(s): G.H. Herling	8. CONTRACT OR GRANT NUMBER(s)
9. PERFORMING ORGANIZATION NAME AND ADDRESS: Naval Research Laboratory, Washington, D. C. 20375	10. PROGRAM ELEMENT, PROJECT, TASK AREA & WORK UNIT NUMBERS: NRL Problem H01-06
11. CONTROLLING OFFICE NAME AND ADDRESS: Department of the Navy, Office of Naval Research, Arlington, Va. 22217	12. REPORT DATE: June 10, 1975
	13. NUMBER OF PAGES: 11
14. MONITORING AGENCY NAME & ADDRESS (if different from Controlling Office)	15. SECURITY CLASS. (of this report): Unclassified
	15a. DECLASSIFICATION/DOWNGRADING SCHEDULE

16. DISTRIBUTION STATEMENT (of this Report)

Approved for public release; distribution unlimited.

17. DISTRIBUTION STATEMENT (of the abstract entered in Block 20, if different from Report)

18. SUPPLEMENTARY NOTES

19. KEY WORDS (Continue on reverse side if necessary and identify by block number)

Dosimetry
Monte Carlo
Neutron dosimetry

20. ABSTRACT (Continue on reverse side if necessary and identify by block number)

Coupled neutron-photon multigroup Monte Carlo transport calculations have been carried out with the code MORSE-CG in a model of the INDI experiment.

UNCLASSIFIED

CONTENTS

MONTE CARLO CALCULATIONS OF NEUTRON AND PHOTON SPECTRA FOR THE INDI PROJECT

INTRODUCTION

Coupled neutron-photon multigroup Monte Carlo transport calculations have been carried out with the code MORSE-CG [1] in a model of the INDI experiment.* The coupled multigroup neutron and photon cross-section data have been obtained from the CASK library [2], which is based on data contained in the ENDF/B-II and ENDF/B-III evaluations.

The continuous energy variable E is replaced, in the multigroup method, by a number of discrete energy "groups" of finite width ΔE_g, and to each of which there corresponds a mean energy $\bar{E}_g$. The energy bins, contained in Tables 1 and 2, are generally sums over such energy groups. Angular distributions contained in the library are represented in terms of the first four terms of a Legendre series (P_0 through P_3), and the uppermost energy of the library is 15 MeV.

Table 1

Neutron energy bin structure. The upper (lower) limit of the energy bin given in the first column is E_u (E_ℓ). The average bin energy is $\bar{E}$, and energy width of the bin is ΔE.

Bin	E_u (MeV)	E_ℓ (MeV)	$\bar{E}$ (MeV)	ΔE (MeV)
1	15.0	12.2	13.6	2.8
2	12.2	8.18	10.1	4.02
3	8.18	1.11	3.69	7.07
4	1.11	2.9×10^{-5}	0.184	1.11
5	2.9×10^{-5}	1.0×10^{-8}	5.45×10^{-6}	2.9×10^{-5}

Table 2

Photon energy bin structure. The column headings have the same meanings as in Table 1.

Bin	E_u (MeV)	E_ℓ (MeV)	$\bar{E}$ (MeV)	ΔE (MeV)
1	10.0	4.0	6.62	6.0
2	4.0	2.0	2.83	2.0
3	2.0	1.33	1.66	0.67
4	1.33	0.30	0.723	1.03
5	0.30	1.0×10^{-2}	0.126	0.29

*International Neutron Dosimetry Intercomparison (INDI) under the sponsorship of the International Commission on Radiation Units and Measurements.

Note: Manuscript Submitted March 17, 1975.

CALCULATION MODEL

Phantom Model

The effects of room air, other background scattering, the phantom walls, etc. have been neglected throughout the calculations. The 30-cm-cube water phantom has been replaced by a 16.926-cm-radius, 30-cm-long cylinder. At each depth, an assumed point detector has been surrounded by a coaxial cylindrical void of radius 0.5 cm and length 1.0 cm, with the detector at the center. The purpose of the void is discussed in connection with the flux estimation. The results at the three depths of 5, 10, and 20 cm have been obtained separately, so that only one such void is present in any calculation.

The phantom geometry and its relation to the RARAF* source are illustrated in Fig. 1.

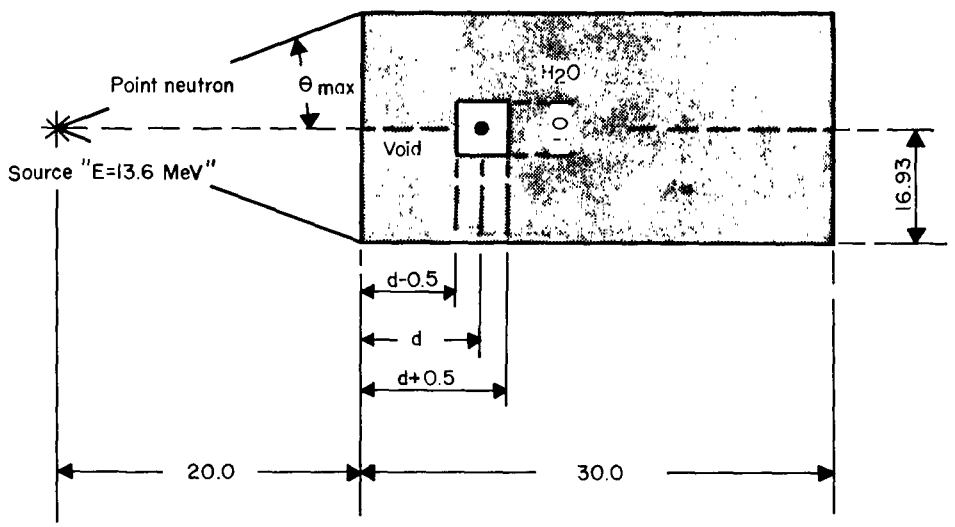

Fig. 1 — The phantom geometry of the calculations in relation to the RARAF source as viewed normal to the axis of cylindrical symmetry. Lengths are in centimeters.

Source Model

Because the highest energy neutron group of the cross-section library covers the range 15 MeV $\geqslant E_n >$ 12.2 MeV, the 15.5-MeV RARAF source [3] has been replaced by a neutron source having an energy of 13.6 MeV. The highest energy neutrons of the model are, therefore, expected to predict a somewhat lower kerma than that observed experimentally.

*Radiological Research Accelerator Facility (RARAF), Brookhaven National Laboratory.

The isotropic angular distribution of the neutron source has been replaced by an angular distribution which is isotropic within the cone defined by the solid angle subtended by the irradiated face of the phantom at the source point, $\Delta\Omega_{max} = 2\pi\,(1 - \cos\theta_{max})$. The remainder of the beam has been neglected in accordance with the approximations of the preceding sub-section.

Flux Estimation

Both the neutron and photon spectra have been calculated by estimating the flux at a point for each detector point.

In Fig. 2a, the heavy solid line represents part of, for example, the history of a neutron as it traverses the phantom, which for the moment is assumed homogeneous. If $\mathbf{r}$ denotes a collision site, indicated by a vertex of the figure, $\mathbf{R}_D$ a detector point, and $\vec{\Omega}$ the unit vector $(\mathbf{R}_D - \mathbf{r})/|\mathbf{R}_D - \mathbf{r}|$ expressed in a coordinate system centered at the collision site and oriented along the neutron direction before collision, the expected contribution appearing at the detector is given by

$$dn = w \exp(-\mu|\mathbf{R}_D - \mathbf{r}|)P(\mathbf{\Omega})\, d\,\mathbf{\Omega}, \tag{1}$$

where w is the weight of the outgoing neutron, μ is the narrow-beam attenuation coefficient corresponding to the outgoing neutron energy, and $P(\vec{\Omega})$ is the normalized angular distribution of the outgoing neutrons. Consideration of an infinitesimal area centered at the detector point, as in Fig. 2b yields the expected flux at a point

$$dn/dA = w \exp\,(-\mu|\mathbf{R}_D - \mathbf{r}|)P(\mathbf{\Omega})\,(1/|\mathbf{R}_D - \mathbf{r}|^2). \tag{2}$$

This quantity is summed over all collision sites as indicated by the dashed lines in Fig. 2a, and averaged over all histories in order to yield the final flux estimate. The role of the void is to ensure that Eq. (2) remains finite by eliminating collisions with $\mathbf{r} \approx \mathbf{R}_D$.

The same reasoning may also be applied to the birth of a source neutron with the result

$$(dn/dA)_{source} = 1.0(1/\Delta\Omega_{max}) \exp[-\mu(d - 0.5)]\,[1/(20 + d)^2] \tag{3}$$

for every source particle, where the effect of the void has been taken into account.

Because the source has been assumed to have no photon contaminant, only Eq. (2) applies to photons.

RESULTS

The energy bin structures for neutrons and photons are given in Tables 1 and 2 respectively. Except for the highest energy neutron bin, all bins contain several energy

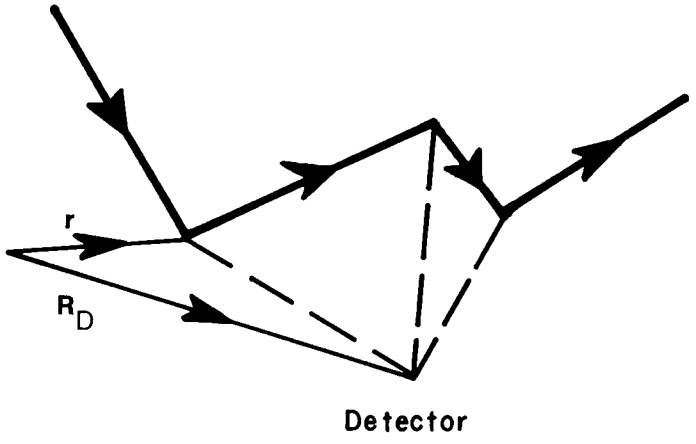

(a) Part of a neutron (photon) history is depicted by the heavy solid lines. The dashed lines indicate a contribution scored according to Eq. (2). The vectors r and R_D denote a collision site and detector point in the overall coordinate system.

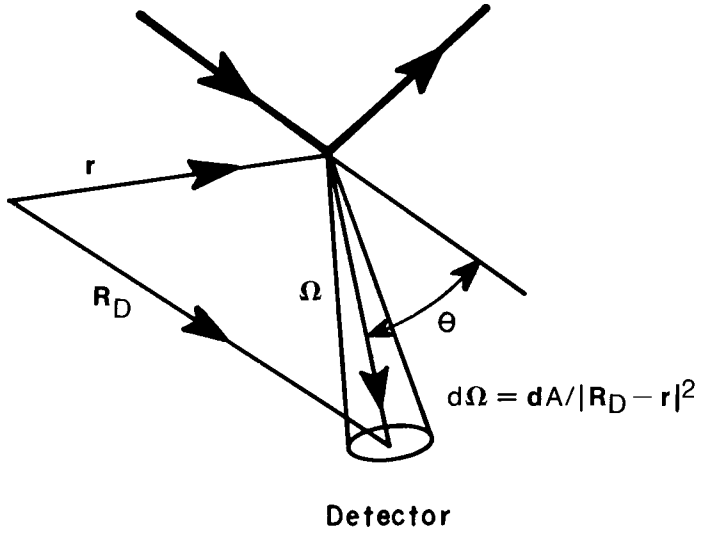

(b) Detailed corresponding to one of the dashed lines in (a), and leading to Eqs. (1) and (2).

Fig. 2 — Estimation of flux at a point.

groups. In both tables, E_u (E_ℓ) is the upper (lower) energy of the bin of which the width is ΔE MeV. The average energy assigned to each neutron bin is the arithmetic mean of the quantities

$$\bar{E}_g = (E_{ug} - E_{\ell g})/ln\,(E_{ug}/E_{\ell g}),$$

which have been calculated for each neutron group belonging to the bin. The average energy assigned to the photon bins is the arithmetic mean over the groups comprising the bin.

The neutron spectra at depths of 5, 10, and 20 cm within the phantom are contained in Tables 3, 5, and 7 respectively, and the corresponding photon spectra are contained in Tables 4, 6, and 8. The second column of these tables contains the average bin energy, and the third column contains the bin width. The fourth column contains the particle flux per unit energy, $\Delta\varphi/\Delta E$, normalized to 10^6 source neutrons, and the fifth column contains $\Delta\varphi = (\Delta\varphi/\Delta E)\Delta E$. The last column contains the fractional standard deviation (fsd) of the fourth column, and represents the statistical error expressed in percent. The fsd of the first neutron bin is particularly small because according to Eq. (3) every source neutron supplies the same contribution to that bin. Thus, the mean value receives a finite contribution at neutron birth, but the variance receives a vanishing contribution. The results at the three depths have been obtained in separate runs, each of which has used 5000 neutron histories.

Table 3

Neutron flux at 5 cm depth. The quantity $(\Delta\varphi/\Delta E)$ is expressed in particles/(cm^2 - MeV - 10^6 source neutrons), and $\Delta\varphi = (\Delta\varphi/\Delta E)\Delta E$ is expressed in particles/(cm^2 - 10^6 source neutrons). The last column contains δ, the fractional standard deviation in $\Delta\varphi/\Delta E$ expressed in percent.

Bin	$\bar{E}$ (MeV)	ΔE (MeV)	$\Delta\varphi/\Delta E$	$\Delta\varphi$	δ (%)
1	13.6	2.8	312	874	7
2	10.1	4.02	28	112	13
3	3.69	7.07	50	350	16
4	0.184	1.11	188	209	36
5	5.45×10^{-6}	2.90×10^{-5}	2.08×10^{7}	603	36

Table 4

Photon flux at 5 cm depth. The column headings have the same meanings as in Table 3.

Bin	$\bar{E}$ (MeV)	ΔE (MeV)	$\Delta\varphi/\Delta E$	$\Delta\varphi$	δ (%)
1	6.62	6.0	12	73	11
2	2.83	2.0	63	126	11
3	1.66	0.67	14	9	18
4	0.723	1.03	34	35	14
5	0.126	0.29	274	79	22

The results contained in Tables 3 through 8 have been employed for the calculation of $R = 100D_\gamma/(D_n + D_\gamma)$ in water at each of the three depths. The neutron kerma, D_n, has been obtained with the help of linear interpolation of kerma-to-fluence ratios [4] to the mean bin energies. The photon kerma has been obtained by applying the relation [5]

Table 5
Neutron flux at 10 cm depth. The column headings have the same meanings as in Table 3.

Bin	$\bar{E}$ (MeV)	ΔE (MeV)	$\Delta\varphi/\Delta E$	$\Delta\varphi$	δ (%)
1	13.6	2.8	142	398	4
2	10.1	4.02	28	110	19
3	3.69	7.07	32	229	24
4	0.184	1.11	346	384	65
5	5.45×10^{-6}	2.90×10^{-5}	1.88×10^{7}	545	48

Table 6
Photon flux at 10 cm depth. The column headings have the same meanings as in Table 3.

Bin	$\bar{E}$ (MeV)	ΔE (MeV)	$\Delta\varphi/\Delta E$	$\Delta\varphi$	δ (%)
1	6.62	6.0	8	47	7
2	2.83	2.0	65	130	7
3	1.66	0.67	30	20	29
4	0.723	1.03	51	53	30
5	0.126	0.29	315	91	22

Table 7
Neutron flux at 20 cm depth. The column headings have the same meanings as in Table 3.

Bin	$\bar{E}$ (MeV)	ΔE (MeV)	$\Delta\varphi/\Delta E$	$\Delta\varphi$	δ (%)
1	13.6	2.8	36	101	7
2	10.1	4.02	15	62	27
3	3.69	7.07	18	130	24
4	0.184	1.11	62	68	42
5	$5.45 \times \cdot 10^{-6}$	2.90×10^{-5}	2.04×10^{7}	592	65

Table 8
Photon flux at 20 cm depth. The column headings have the same meanings as in Table 3.

Bin	$\bar{E}$ (MeV)	ΔE (MeV)	$\Delta\varphi/\Delta E$	$\Delta\varphi$	δ (%)
1	6.62	6.0	4	24	10
2	2.83	2.0	60	120	19
3	1.66	0.67	15	10	20
4	0.72	1.03	22	23	11
5	0.13	0.29	197	57	21

$$D = F(\mu_k/\rho)$$

to each photon bin. The energy fluence, F, has been taken to be

$$F = \bar{E}(\Delta\varphi),$$

and the mass energy transfer coefficients, (μ_k/ρ), have been obtained by linear interpolation of available tables [6]. The values of R thus obtained are given in Table 9, where the calculational error assigned has been computed from the neutron and photon kerma weighted mean errors obtained from the fractional standard deviations.

Table 9
The ratio $R = 100D_\gamma/D_T$ calculated for H_2O.

Depth (cm)	R	
	Calculated	Observed*
5	3.5 ± 0.2	2.5
10	5.4 ± 0.2	≈ 6
20	10.2 ± 0.7	≈10

*Reference 3.

Various refinements of the schematic calculation of the preceding paragraph must, of course, be included for a realistic comparison with a specific experiment. A complete discussion of the application of Tables 1 through 8 to the NRL measurements as a participant in the INDI is reported elsewhere [7].

ACKNOWLEDGMENTS

The author is deeply indebted to Mr. F.H. Attix for bringing this problem to his attention, and for encouragement during the course of the work. He is grateful for illuminating discussions with Dr. E.A. Straker and wishes to thank Miss Anna B. Mays and Mr. S. Podgor for early computational assistance.

REFERENCES

1. E.A. Straker, W.H. Scott, Jr., and N.R. Byrn, RSIC Computer Code Collection, CCC-203, Oak Ridge National Laboratory, 1972.

2. RSIC Data Library Collection, DLC-23, 1974.

3. F.H. Attix, "Report on NRL Measurements at RARAF, Brookhaven National Laboratory, on March 19-22, 1973" (unpublished), private communication.

4. R.L. Bach and R.S. Caswell, Rad. Res. 35, 1 (1968).

5. E. Tochilin and B.W. Shumway, *Radiation Dosimetry*, 2nd edition, Vol. III, F.H. Attix and E. Tochilin, editors, Academic Press, New York, 1969, p. 253.

6. J.H. Hubbell, "Photon Cross Sections, Attenuation Coefficients, and Energy Absorption Coefficients from 10 keV to 100 GeV," NSRDS-NBS 29, 1969.

7. F.H. Attix, R.B. Theus, S.C. Gorbics, and C.C. Rogers, "Report on NRL Measurements as a Participant in the INDI, NRL Memorandum Report 3051, 1975.